Institute Of Engineering, Pulchowk Campus

Tribhuvan University

Acknowledgement

We would like to express our heartfelt gratitude to the Department of Mechanical and Aerospace Engineering at Pulchowk Campus and the Incubation, Innovation, and Entrepreneurship Centre for their incredible support throughout the SRB project. Their provision of essential materials, guidance, and encouragement was crucial to the successful completion of our work. A special thank you goes to Mr. Nishchal Shrestha for his unwavering support and insightful oversight. His assistance in critical aspects of the project made a significant difference. The resources and mentorship provided by everyone helped us overcome challenges and achieve our goals. We are grateful for the role they played in making our project a success.

Abstract

This documentation presents the design, development, and testing of a solid-fuel rocket by Team SRB. The project aimed to achieve an apogee of 3000 meters, incorporating advanced aerodynamic, structural, and avionics systems. A robust recovery mechanism ensured safe retrieval, and a custom-built launch system supported the rocket's stability during takeoff. The project demonstrates the team's ability to integrate engineering principles with hands-on application, contributing valuable insights to model rocketry. Future iterations will focus on optimizing propulsion efficiency and exploring alternative recovery techniques.

Table of Contents

1. Introduction

Rocketry has long been a fundamental aspect of aerospace engineering, facilitating exploration, experimentation, and technological advancements. It enables the investigation of space, supports the testing of innovative technologies, and drives developments that enhance our understanding of the universe.

The development of the Solid Rocket Booster (SRB) was an exciting and challenging project that integrated propulsion, avionics, aerodynamics, and structural engineering. This documentation explains the careful design, manufacturing, and testing steps that helped the rocket reach an impressive apogee of 2550 meters. The propulsion system, powered by a carefully formulated solid fuel, was tested to optimize burn rates, chamber pressure, and thrust efficiency. In avionics, a transmitter module equipped with a Teensy 4.1 microcontroller, GPS, barometric and inertial sensors, and a LoRa communication system ensured accurate data acquisition, real-time monitoring, and dual-parachute deployment for recovery. Ground-based receiver systems also helped ensure the reliability and precision of the project.

1.1.Objective

1)To design, build and test a solid rocket booster capable of achieving an apogee of 3000 meters.

2)To successfully recover the built rocket and acquire data for future tests and fabrication.

3)To foster future innovations avoiding previously encountered mistakes and providing proper recommendations.

1.2.Background

The SRBs are the largest solid propellant rocket motors ever flown, and the first designed for reuse. A Solid Rocket Booster (SRB) is a type of propulsion system that utilizes solid propellants to produce thrust. These boosters are essential components of many rocket designs, as they provide the crucial initial thrust needed to lift the vehicle off the ground and support its ascent during the early phases of flight. By delivering a powerful and reliable source of propulsion, SRBs help ensure that the rocket can overcome the forces of gravity and gain the necessary speed to continue its journey into space.

SRB operates based on Newton's Third Law of Motion, which states that "for every action, there is an equal and opposite reaction." When the solid propellant within the booster is ignited, it generates high-pressure gases. These gases are directed through a nozzle, creating thrust that propels the rocket upward.[1] This fundamental principle of physics is what enables the SRB to effectively lift the vehicle off the ground and into the air, playing a crucial role in the launch process.

Solid Rocket Boosters provide greater thrust without significant refrigeration and insulation requirements and produce large amounts of thrust for their size. Adding detachable SRBs to a vehicle also powered by liquid-propelled rockets known as staging reduces the amount of liquid propellant needed.[2] Solid boosters are cheaper to design, test, and produce in the long run compared to the equivalent liquid propellant boosters.

Solid Rocket Boosters (SRBs) are commonly utilized in launch vehicles for both orbital and suborbital missions. They serve as auxiliary boosters, delivering the necessary initial thrust required for heavy-lift rockets. Notable examples include NASA's Space Shuttle and the Ariane 5, where SRBs play a critical role in enhancing the overall launch capability and ensuring successful liftoff. Their reliability and efficiency make them a key component in modern rocket design.

In our project, the Solid Rocket Booster (SRB) functions as the primary propulsion system, enabling the rocket to reach an impressive apogee of 3000 meters. Our SRB design features advanced propellant formulations and optimized nozzle geometry, which work together to enhance performance and ensure efficient thrust generation. This careful consideration of design elements is crucial for maximizing the rocket's capabilities during its ascent.

This project was initiated as a step toward understanding and applying engineering principles in the design, construction, and testing of a high-performance solid-fuel rocket. The rocket features an integrated solid propulsion system, which provides reliable thrust, along with advanced avionics designed for comprehensive flight data acquisition. This ensures precise monitoring and analysis of flight performance throughout the mission. Additionally, the rocket incorporates a dual-parachute recovery mechanism, enhancing safety and recovery reliability upon descent. The structural design emphasizes durability and aerodynamic efficiency, allowing for stable flight performance under various conditions. This approach aims to achieve successful launches.

This project represents a significant milestone for Team SRB, providing valuable practical experience in the field of aerospace engineering. It offers team members the opportunity to engage directly with the complexities of model rocketry design and testing, fostering a deeper understanding of the engineering principles at play. Moreover, the insights gained throughout this project are not only instrumental in refining our current designs but also serve as a robust foundation for future advancements in propulsion, recovery, and flight systems. By addressing the challenges encountered during development and testing, we aim to enhance our knowledge and capabilities, paving the way for innovative solutions and improvements in subsequent projects. This endeavor reinforces our commitment to excellence in aerospace engineering and contributes to the broader field of rocketry.

Team SRB is a dynamic group of passionate aerospace engineering students from Pulchowk Campus. Our mission is to design, build, and test rockets, pushing the boundaries of student

innovation and technical expertise. Within the team, the works have been divided into four major units with all members handling their work of interest:

- **Structural Team:** Ensures the rocket's frame can withstand forces during flight and landing.
- **Propulsion Team:** Focuses on the design and testing of the solid rocket booster and its performance.
- **Aerodynamics Team:** Handles the rocket's shape, stability, and flight characteristics.
- **Avionics Team:** Designs and implements the electronic systems, including sensors and data acquisition.

Structurally, the rocket was designed using polyester resin, fiber glass, and carefully calibrated catalyst ratios to achieve strength and lightweight durability. Key components such as the body tube, couplers, and nose cone were fabricated through extensive trials involving different material configurations and mold designs. Aerodynamic optimizations minimized drag and ensured stability during flight, confirmed through simulations and experimental tests. The launch controller, featuring a dual-switch ignition mechanism and continuity checks, prioritized safety and functionality throughout the launch process.

This report provides a comprehensive overview of the design, construction, and testing phases of the rocket, serving as a detailed documentation of our project's journey. It encompasses an in-depth analysis of critical components including propulsion systems, aerodynamics, structural integrity, avionics, recovery systems, and the launch setup. Each of these elements is examined to understand their contributions to the overall performance and reliability of the rocket.

Additionally, the report discusses the results obtained from both static and flight tests, offering insights into the rocket's operational capabilities and performance metrics. These results are analyzed in the context of theoretical expectations and practical outcomes, allowing for the understanding of the rocket's behavior during various stages of its mission.

Furthermore, the report highlights the lessons learned throughout the project, emphasizing the importance of iterative design and testing processes. It also identifies potential areas for improvement, providing recommendations for future projects that could enhance performance and efficiency. This thorough analysis not only contributes to our current understanding but also lays the groundwork for continued innovation in rocketry and aerospace engineering.

2. Methods and methodologies

As mentioned earlier, the works have been divided into four major units; Structure, Propulsion, Aerodynamics and Avionics. In this section we take a detailed look at what each unit did for developing the 2 meters rocket followed by a separate section on recovery works, launch stand and launch controller.

However, before the actual works of the final body it was important to go through different simulations and finalize the components.

2.1. Rocket Design and Performance Analysis Using OpenRocket

The primary objective of this project was to design a model rocket capable of reaching an apogee of 3000 meters. To achieve this, the design process began with the selection and definition of key parameters, including the rocket's diameter, nose cone shape, and fin configuration. The total length of the rocket was set at approximately 2 meters, ensuring the inclusion of all necessary components in the design.

An initial design was created using OpenRocket, incorporating calculated specifications to meet the target apogee. A solid rocket motor was selected and simulated in OpenRocket to determine its compatibility with the design. The simulation results provided an estimated apogee, which validated the chosen motor class for the rocket.

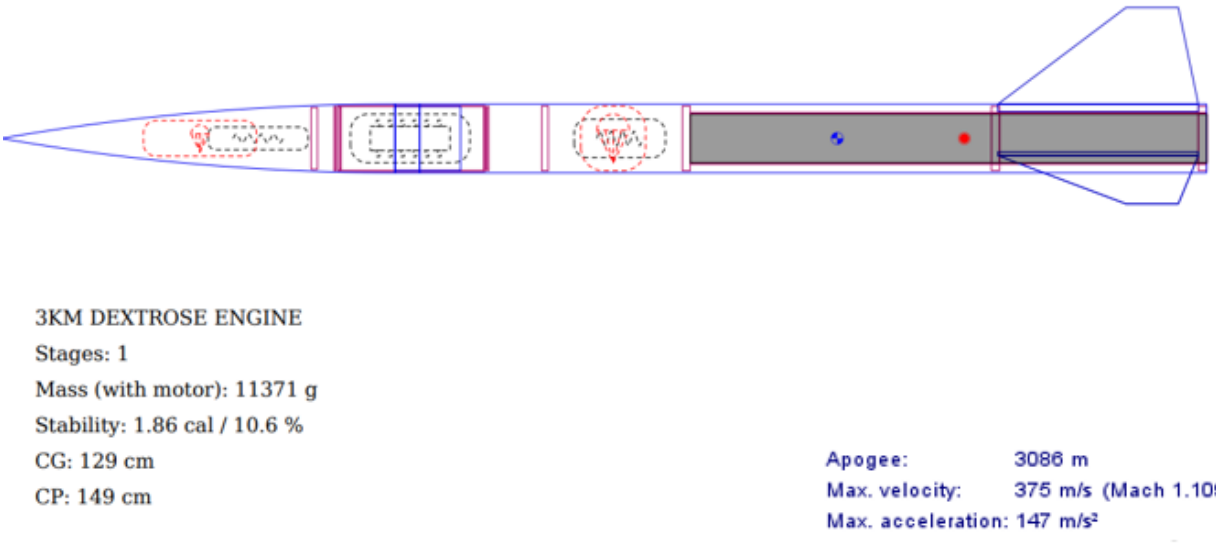

Figure 2.1.1: rocket design and key parameters with simulated motor

Following the initial simulations, a static test of the selected motor was conducted to verify its performance against the simulated data. The test results were satisfying, demonstrating close

alignment with the simulated apogee predictions. This successful validation of the motor's performance allowed the project to proceed to the fabrication stage.

3KM DEXTROSE ENGINE
Stages: 1
Mass (with motor): 13040 g
Stability: 1.58 cal / 8.23 %
CG: 145 cm
CP: 161 cm

Apogee: 2603 m
Max. velocity: 281 m/s (Mach 0.829)
Max. acceleration: 122 m/s²

Figure 2.1.2: rocket design and key parameters with a ground tested motor

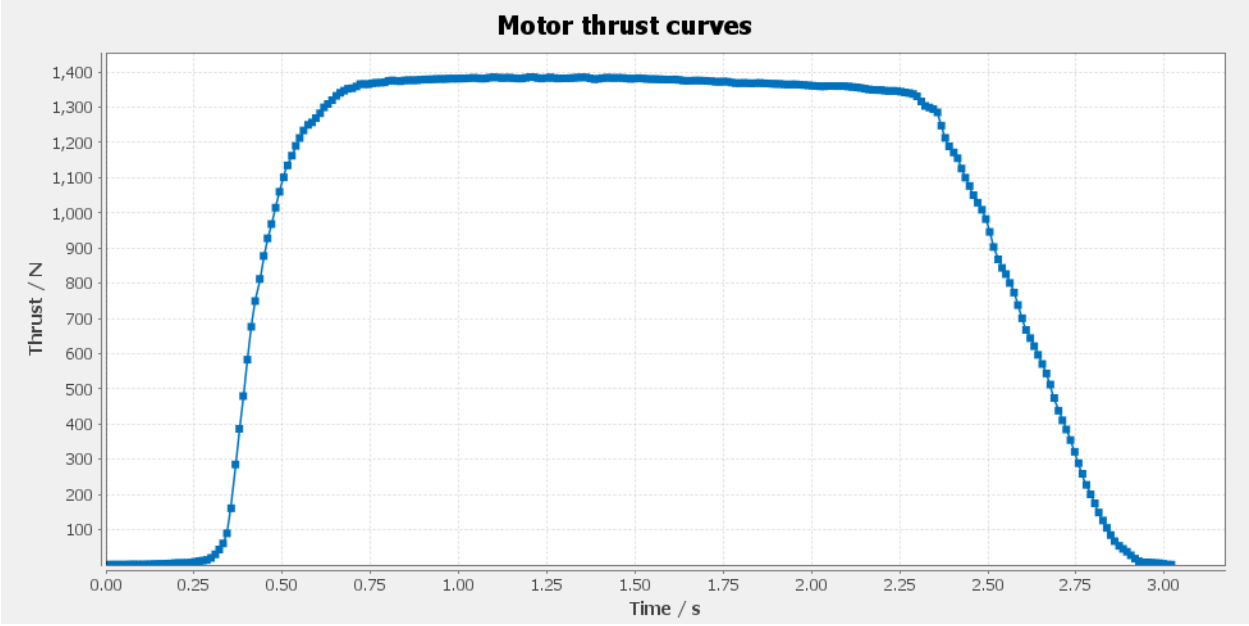

Common name:	L2583
Total impulse:	2972 Ns (16% L)
Avg. thrust:	1176 N
Max. thrust:	1386 N
Burn time:	2.52 s
Launch mass:	7404 g
Empty mass:	4500 g

Fig 2.1.3: Results of a first static test

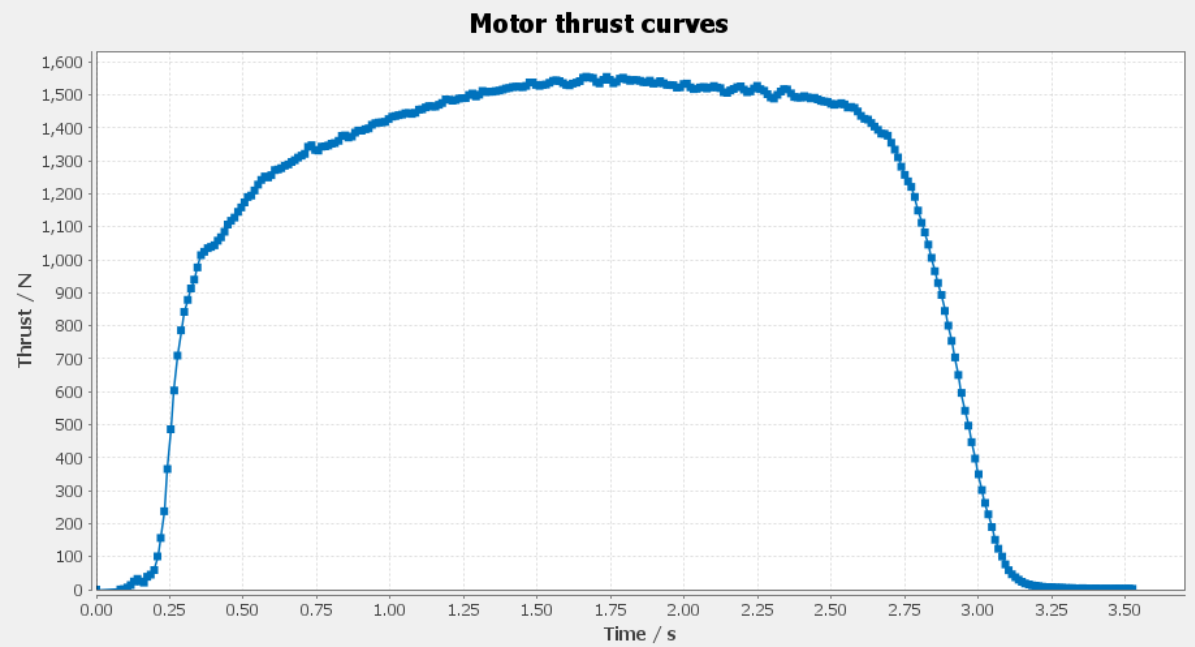

Common name:	L2583
Total impulse:	3775 Ns (47% L)
Avg. thrust:	1304 N
Max. thrust:	1555 N
Burn time:	2.89 s
Launch mass:	8560 g
Empty mass:	5462 g
Motor type:	Unknown

Fig 2.1.4: Results of second static test

The results obtained from a static test of motor were satisfactory and also consistent which is presented in figure 2.1.3 and 2.1.4. The impulse, peak thrust and burn time were all obtained better in the second test in comparison to that of the first test. The mass and density of propellant played a significant role. So, with proper weighing and casting of propellant, better results were obtained in the second static test of the motor.

Comparison of simulated motor and tested motor

Description	*Data of simulated motor*	*Data of first static test*	*Data of second static test*
Total impulse	4169 Ns	2972 Ns	3775 Ns
Average thrust	1480 N	1176 N	1304 N
Peak thrust	1550 N	1386 N	1555 N
Burn time	2.82 s	2.52 s	2.89 s
Launch mass	6502 g	7404 g	8560 g
Empty mass	2490 g	4500 g	5462 g

Major changes were seen in overall rocket performance due to these differences in simulated and tested motor. The changes in key parameters are visible in figure 2.1.1 and figure 2.1.2.

Once the static test of motor was completed, the fabrication of the rocket's body parts began. Each component was carefully manufactured and weighed to ensure precision. These updated weight values were once again incorporated into the OpenRocket model to refine the simulations and obtain more accurate predictions for the rocket's apogee and stability.

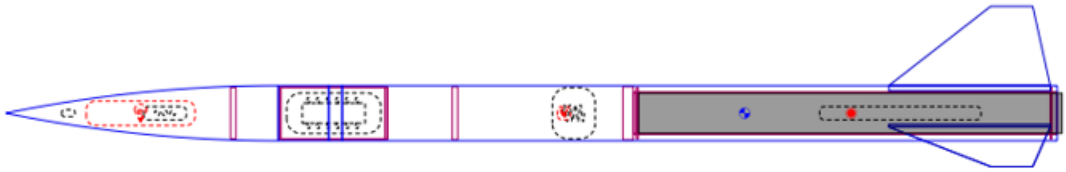

Motor Eater
Stages: 1
Mass (with motor): 14413 g
Stability: 1.94 cal / 10.1 %
CG: 139 cm
CP: 160 cm

Apogee: 2577 m
Max. velocity: 255 m/s (Mach 0.752)
Max. acceleration: 110 m/s²

Figure 2.1.5: rocket design and key parameters after the fabrication of each part and their actual weight updated on open rocket with a ground tested motor

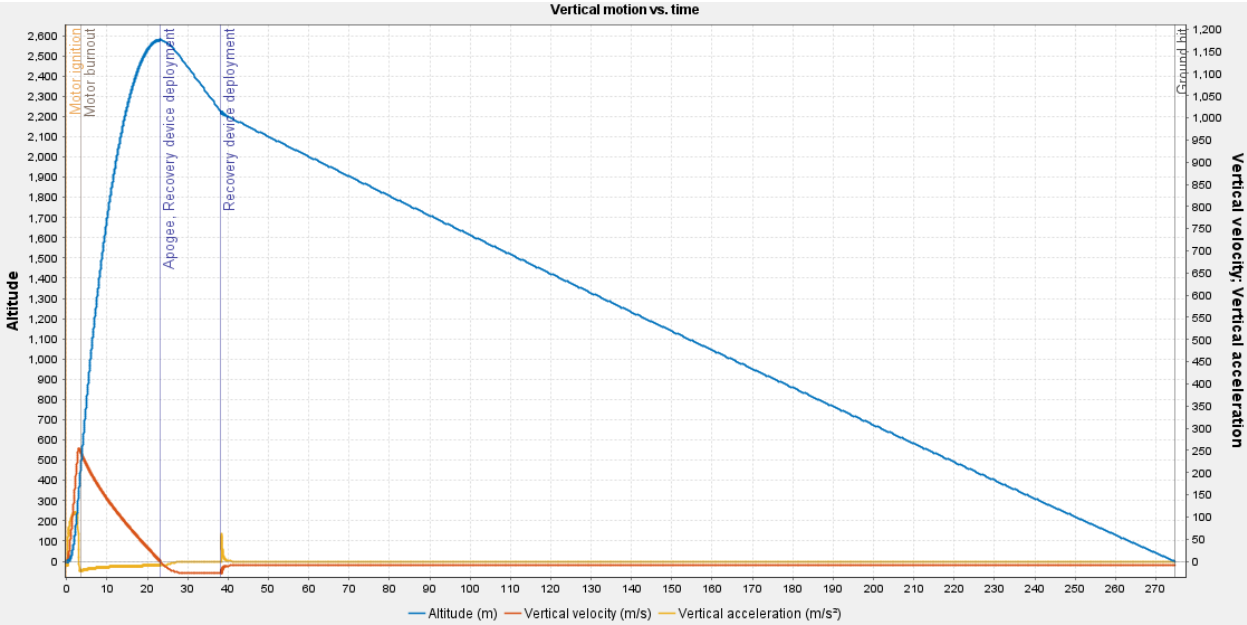

Figure 2.1.6: graph of vertical motion vs time simulated by open rocket

2.2. Structure construction

The structural design of the rocket is one of the most critical aspects of ensuring its performance and safety during flight. At SRB, we developed the structural components of the rocket through a series of trials and innovations. The primary materials used in our rocket's structure were resin and fiberglass, carefully selected and tested for optimal performance.

We evaluated two types of resins—polyester resin and epoxy resin—and chose polyester resin for its cost-effectiveness and suitability for our applications. The process required the use of cobalt as a catalyst and a hardener. Initially, we bought resin with cobalt already mixed, which was purple in color. However, the exact proportion of cobalt was unknown, leading to challenges in determining the appropriate hardener ratio. To address this, we conducted patch tests with varying proportions of hardener to find the optimal mix. The results we got were okay but despite our efforts, the results were quite inconsistent. Eventually, we transitioned to purchasing resin with a lower cobalt content and repeated the testing process, but this too proved quite insufficient.

Finally, we purchased resin without any cobalt pre-mixed, enabling us to experiment and fine-tune the ratio of cobalt and hardener precisely. After numerous trials, we determined that the ideal proportions were **0.5% cobalt** and **1–2% hardener**, depending on the desired curing speed. These ratios were calculated relative to the amount of resin used.

Fiberglass served as the reinforcement material for all structural components. We tested fiberglass of various GSM (grams per square meter) to determine the most suitable grade for each part. After extensive testing, **300 GSM** and **450 GSM** fiberglass were selected for their balance of strength and flexibility. These were used for components such as the coupler, body tube, casting tube, liner, and nose cone. For critical parts like the body tube and nose cone, additional layers of fiberglass cloth were applied to ensure enhanced durability.

Each structural component required a custom mold. These molds were prepared by layering them with chart paper and tape to ensure the desired dimensions and to prevent resin seepage. Careful attention was given to maintain the molds' surface quality, making the extraction process easier and preserving the structural integrity of the final product.

During fabrication, we experimented with multiple application methods, including applying resin above the fiberglass cloth or pre-soaking the cloth with resin before laying it on the mold. The final method involved layering resin and fiberglass alternately for even distribution and strength.

Brushes were another crucial tool in the manufacturing process, but they were prone to hardening due to resin exposure. To optimize costs, we developed methods for cleaning and reusing brushes by soaking them in thinner. In later stages, started fabricating multiple components simultaneously, using the same brushes across different molds to reduce waste and save resources.

Through iterative testing and innovative practices, we achieved robust and lightweight structural components capable of withstanding the forces experienced during launch and flight.

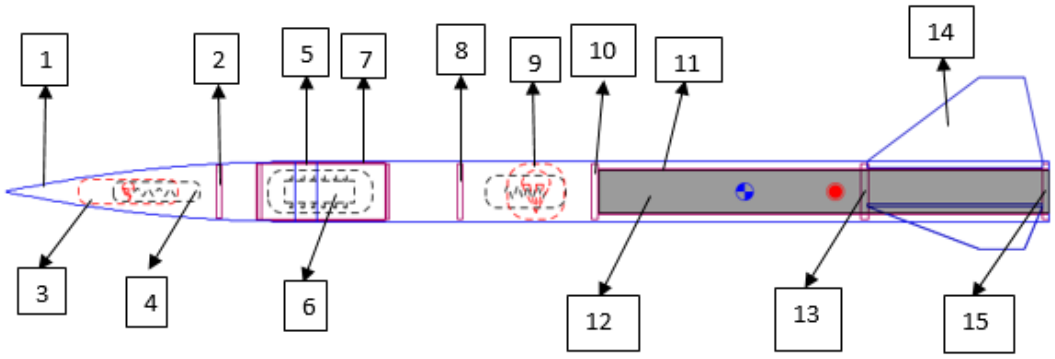

Figure 2.2: Open rocket model representing all parts/components

Overall the list of things we finalized and fabricated for constructing the final body of the project are as follows

The parts/components are listed below in reference to the above picture

S.N	Description
1	Nose cone
2	Separation plate
3	Main parachute
4	Shock cord
5	Vent band
6	Flight computer +sensors +battery
7	Coupler
8	Separation plate
9	Drogue parachute
10	Engine block
11	Motor mount
12	Rocket motor
13	Centering ring
14	Fins
15	Motor retainer

2.2.1. Nose cone

The nose cone material was constructed using fiberglass reinforced with polyester resin. A 450 gsm fiberglass mat was used as the first layer, providing a strong base. A second layer of fiberglass cloth was then added to increase the body's strength and ability to withstand the heat and pressure of flight.

To enhance its performance and durability, the nose cone incorporates a nylon tip and an aluminum tip for effective heat dissipation during high-speed flight (Mach heating).

The avionics bay, along with the parachute system, is housed within the nose cone. To withstand the significant pressures encountered during ejection and the elevated temperatures experienced during flight, fiberglass reinforced polymer (FRP) was chosen as the primary material. FRP offers a favorable combination of high strength-to-weight ratio, excellent resistance to heat and pressure, and good formability, making it an ideal choice for this critical component.

Fig 2.2.1.1 :Final nose cone;

Fig 2.2.1.2 :nylon tip for nose cone

Fig 2.2.1.3 : aluminium tip for nose cone

Mold preparation:

For the preparation of the nose cone mold, we initially attempted to utilize a 3D printed mold. However, this approach proved unsuccessful in achieving the desired level of accuracy and surface finish. As an alternative, we opted for a thermocol foam mold. This involved carefully shaping the thermocol foam to match the required nose cone contours. To achieve the necessary precision, we employed a custom-built hot wire cutter. This tool, fabricated in-house, enabled us to precisely cut and shape the thermocol foam, resulting in a mold with the desired accuracy and smoothness.

Fig2.2.1.4: Nose cone mold

Fig 2.2.1.5: Setup for smoothing of nose cone

Fig 2.2.1.6: Failed nose cone model

2.2.2. Body Tube

The rocket body was constructed using fiberglass reinforced with polyester resin. A 450 gsm fiberglass mat was used as the first layer, providing a strong base. A second layer of fiberglass cloth was then added to increase the body's strength and ability to withstand the heat and pressure of flight.

Mold preparation:
Creating the mold for the 10.2 cm diameter rocket body presented a challenge. Standard PVC pipes with this exact diameter were not readily available. To overcome this, we devised a unique solution. We cut several circular discs with the required diameter and stacked them together to form a cylindrical core. This core was then wrapped with a layer of flex, followed by paper and tape, to create a smooth and consistent surface for the mold.

Fig 2.2.2.: Circular ring stack in set of three with help of double sided tape to maintain same distance

2.2.3. Coupler

The same fiberglass and resin materials were used to construct the coupler. A similar mold-making technique was employed, involving stacking circular discs and wrapping them with flexible material and paper tape. However, to ensure a smooth and seamless finish for the rocket body, a vent was incorporated into the coupler mold. This vent helped to make the finished rocket body with a smooth finish.

Fig 2.2.3.1: Final Coupler with vent.

2.2.4. Fins

Our fins were made from fiberglass sheets of 450 gsm, total 5 layers of those sheets reinforced by polyester resin. The fins had trapezoidal shape with thickness 0.4763cm, tip chord 10 cm, root chord 31 cm, height 11.31 cm and sweep length, 19.2 cm.The complete fin structure involves a mounting tube of length 70.8 cm, outer diameter 7.94 cm and inner diameter of 7.62 cm. The fins were attached on the outer surface of the mounting tube with the help of Araldite which is an epoxy-based adhesive.

Fig 2.2.4.1: fins attached to mounting tube

In order to get our final fins, we used a rectangular plywood piece and vacuum bags. We marked a rectangular outline on the plywood piece and cut fiberglass sheets of same dimensions (5 sheets per fin). Then, we started applying resin on one sheet and before it could set, we layered another sheet on top; we repeated the same process for 5 sheets. Once we were done applying resin, we immediately pressed another plywood piece on top of the fiberglass and put this entire thing inside vacuum bags. Vacuum bags were used to ensure that no air bubbles would form and additional weight was also put on top of the bags for extra pressure.

The bags were opened next day when the resin was all set, the slab of resin reinforced fiberglass was taken and both upper and lower surfaces were smoothened out with the use of a grinder. Once we get the desired smoothness and thickness of the slab, an outline of the fin structure was marked and precisely cut. Chamfering was done on the edges of the fins with a set up built by our team out of plywood and hand grinder. With this, our fins were obtained and were attached to the mounting tube.

To fix the mounting tube inside the body tube first, we marked and created slots on the body tube through which fins are supposed to protrude. Then, we carefully inserted the mounting tube inside the body tube and used the same epoxy-based adhesive to fix the fins to the outer surface of body tube as well as to give filleted corners at the joints. The mounting tube was fixed in a stable manner with the help of multiple centering rings that were 3D printed. This is how we made and attached fins to the body. Finally, we reinforce the fins with fiber cloth and resin (tip to tip reinforcement) for additional smoothness and strength. For this, three large pieces of fiber cloth were cut in a way that they cover the entire portion of two surfaces from two fins and portion of body tube between them with lots of excess cloth for tolerance. Once this was set, lots of hand sanding had to be done with sandpaper to get the final tip to tip reinforced fins.

2.2.5. Flutter Analysis

We performed a flutter analysis for the fins using the values of root chord, tip chord, semi span, fin thickness and height of maximum velocity. We did the analysis of fin flutter velocity using Martin's method.

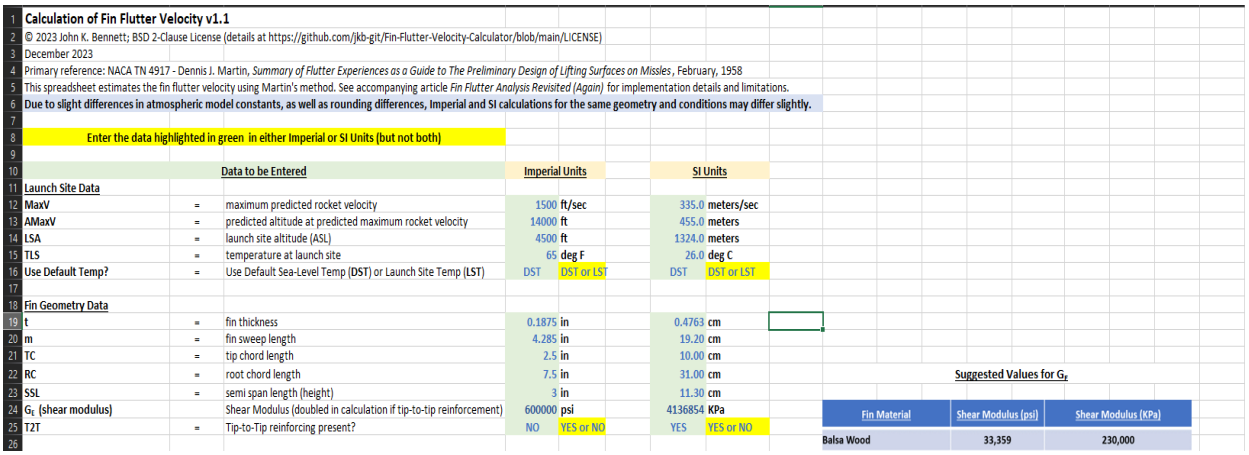

Calculation of Fin Flutter Velocity v1.1

© 2023 John K. Bennett; BSD 2-Clause License (details at https://github.com/jkb-git/Fin-Flutter-Velocity-Calculator/blob/main/LICENSE)

December 2023

Primary reference: NACA TN 4917 - Dennis J. Martin, *Summary of Flutter Experiences as a Guide to The Preliminary Design of Lifting Surfaces on Missles*, February, 1958

This spreadsheet estimates the fin flutter velocity using Martin's method. See accompanying article *Fin Flutter Analysis Revisited (Again)* for implementation details and limitations.

Due to slight differences in atmospheric model constants, as well as rounding differences, Imperial and SI calculations for the same geometry and conditions may differ slightly.

Enter the data highlighted in green in either Imperial or SI Units (but not both)

Data to be Entered			Imperial Units		SI Units	
Launch Site Data						
MaxV	=	maximum predicted rocket velocity	1500	ft/sec	335.0	meters/sec
AMaxV	=	predicted altitude at predicted maximum rocket velocity	14000	ft	455.0	meters
LSA	=	launch site altitude (ASL)	4500	ft	1324.0	meters
TLS	=	temperature at launch site	65	deg F	26.0	deg C
Use Default Temp?	=	Use Default Sea-Level Temp (DST) or Launch Site Temp (LST)	DST	DST or LST	DST	DST or LST
Fin Geometry Data						
t	=	fin thickness	0.1875	in	0.4763	cm
m	=	fin sweep length	4.285	in	19.20	cm
TC	=	tip chord length	2.5	in	10.00	cm
RC	=	root chord length	7.5	in	31.00	cm
SSL	=	semi span length (height)	3	in	11.30	cm
G_E (shear modulus)		Shear Modulus (doubled in calculation if tip-to-tip reinforcement)	600000	psi	4136854	KPa
T2T	=	Tip-to-Tip reinforcing present?	NO	YES or NO	YES	YES or NO

Suggested Values for G_E

Fin Material	Shear Modulus (psi)	Shear Modulus (KPa)
Balsa Wood	33,359	230,000
Birch Aircraft Plywood	89,000	613,633
G10 & G12 Epoxy Fiberglass	600,000	4,136,854
Carbon Fiber Epoxy Composite	600,000	4,136,854
6061-T6 Aluminum	3,800,000	26,200,078
Ti-6Al-4V Titanium	6,200,000	42,747,495
4130 Steel	12,000,000	82,737,087

Calculated Values					
Cx (for trapezoidal fins) (edit formula for other fin shapes)	$C_x = \frac{(2\times TC\times m)+TC^2+(m\times RC)+(TC\times RC)+RC^2}{3(TC+RC)}$	4.49	in	19.11	cm
t/c (thickness ratio)	fin thickness / root chord length	0.0250		0.0154	
λ (lambda) (taper ratio) (create "pseudo" tip chord if nec.)	tip chord length / root chord length	0.3333		0.3226	
Fin Area (trapezoidal fin) (edit formula for other fin shapes)	$Area = Height\times\frac{Tip\ Chord\ Length+Root\ Chord\ Length}{2}$	15.000	in sq	231.650	cm sq
A (aspect ratio)	(semi-span length or height)^2 / fin area	0.6000		0.5512	
ε (epsilon)	$\varepsilon=(\frac{C_x}{RC})-0.25$	0.3492		0.3664	
DN (denominator constant)	$DN=\frac{(24\times\varepsilon\times\kappa\times p_0)}{\pi}$	54.88	psi	397.03	KPa
Tf or Tc (air temp at AMaxV)	$T_C = 15-(.0065\times altitude_{meters})$	-6.86	deg F	3.44	deg C
	$T_F = 59-(.00356\times altitude_{ft})$				
a (speed of sound at AMaxV)	$a_{m/sec}=20.05\times\sqrt{273.16+T_C}$	1043.36	ft/sec	333.46	meters/sec
	$a_{ft/sec}=49.03\times\sqrt{459.7+T_F}$				
p (air pressure at AMaxV)	$P_{(psi)}=14.696\times(\frac{T_F+459.7}{518.7})^{5.256}$	7.20	psi	81.70	KPa
	$P_{(KPa)}=101.325\times(\frac{T_C+273.16}{288.16})^{5.256}$				
First Term	$\frac{DN\times A^3}{(\frac{L}{c})^3\times(A+2)}$	291797.59	psi	7188298.59	KPa
Second Term	$(\frac{\lambda+1}{2})$	0.67		0.66	
Third Term	$(\frac{p}{p_0})$	0.49		0.81	
Vf	$V_f = a\times\sqrt{\frac{G_E}{\frac{DN\times A^3}{(\frac{L}{c})^3\times(A+2)}\times(\frac{\lambda+1}{2})\times(\frac{p}{p_0})}}$	2618.13	ft/sec	489.92	meters/sec
Safety Margin		1118.1	ft/sec	154.9	meters/sec
Safety Margin %	>= 25% margin is good; 20-25% margin is fly-with-caution; and < 20% margin is no-fly	74.5	%	46.2	%

We used the excel sheet available online in rocketry forums and edited the fin parameters with those of our fin design. That is how we got the flutter velocity i.e.; 489.92 meters/sec. The safety margin for a safe flight needs to be more than 25%, 20% -25% is where flights are allowed but with high caution and below 20% is a no flight condition. In our analysis, the safety margin was 46.2% which ensured a safe flight.

Fig 2.2.5.1: fin flutter analysis using Martin's method

Note: We can see a column in the excel sheet that shows 74.5% safety margin; this is the column for calculations in imperial units. This difference is caused due to slight differences in atmospheric modal constants and rounding differences in all the values and calculation.

2.2.6. Motor Liner

The motor liner used in our rocket was made from resin reinforced fiberglass. We experimented with fiberglass sheets of 300 gsm and 450 gsm to see which one would be best suited for the final product. Let's first discuss about the mold preparation for liner. The first few samples were made on a mold of metal pipe wrapped by flex multiple rounds to get desired diameter with a layer of tape to avoid bonding of resin with the flex. This method took a lot of time to prepare the mold and a lot of effort to take the liner out of the mold. In this method. the flex used for mold would be useless after only one use so we had to improvise.

The mold we prepared after was made from a plastic pipe of very thick walls. The final mold was prepared on a lathe machine using external turning process in which we remove the external excess part of the pipe to get desired diameter. The mold had a length of only 70 cm and it was divided into two pieces from the middle which could help us to easily remove the liner from the mold.

Once we get the final mold, we wrap a large piece of paper on the surface tightly with minimal overlap and tape the paper in circles around the circumference. We had to make sure not to leave any gaps through which resin could reach the paper and bond with it. Then, we take a large sheet of fiberglass that could wrap around the mold in a single piece without large overlap and apply resin on it evenly until it is completely soaked. Then we let the resin set for some hours and once it hardens, we take out the liner in a single piece by pulling and twisting on both ends. The extracted liner is smoothened out on outer surface with the help of hand grinder and we get the final liner.

As mentioned before, we had done experiments with fiberglass of different gsm. We had to do that because first few liners made with 450 gsm sheet were too thick which required a lot of grinding to reduce the outer diameter. It was labor heavy so we started using 300 gsm sheet which were relatively thinner and had enough rigidity as required for the final product. However, the liner made from 300 gsm had to be made as perfectly as possible because its lesser thickness made it difficult to grind it for smoothening the imperfections on the outer surface. After making multiple samples from 300 gsm, not many of them could be an option for the final product as they would have a lot imperfections such as holes caused by air bubbles and flexible body caused by its too thin walls. Due to these issues, we had to go back to using 450 gsm sheets as they gave better final products despite being labor heavy.

Fig 2.2.6.1: Motor liner

Fig 2.2.6.2: Liner mold

2.2.7. Casting Tube

Like many other of our components, casting tubes were also made from resin reinforces fiberglass of 450 gsm. The mold of the casting tube was made in a similar way as that of the liner; by external turning of a large block of wood in the lathe until we got a block of desired diameter and length and we added a handle in this mold for easy removal of the tube.

Fig 2.2.7.1: mold for casting tube under processing

The technique used for preparing the mold and applying resin is the same as the liner. First, we take a piece of paper that we wrap around the mold tightly without big overlap and tape the paper along the circumference in circular pattern without leaving any gaps that exposes paper. Then, we take a piece of fiberglass that is of length 18 cm at least and wraps around the circumference with no gap and huge overlap. Then we apply resin on the sheet until it is completely soaked and leave the resin to set. Once it sets, we cut the edges off of the taped paper for easy removal of the tubes. The tubes are then sanded down till they fit firmly inside the liner and their length is cut off to 13.2 cm which is the length of the final product.

Fig 2.2.7.2: Casting tube

fig2.2.7.3: Casting tube mold

2.2.8. Resin Preparation

Preparing resin for reinforcement on fiberglass requires us to mix cobalt (6%) into the polyester resin. The volume of cobalt used is 0.5% of the volume of resin. After mixing the cobalt, we use hardener to start the reaction which slowly sets the resin. The time required for the resin to set depends on the quantity of hardener used and which is generally 1.5% of the volume of the resin used.

Experiments on resin:

In the very first days, we used to prepare resin in a volumetric manner i.e., the quantity of all the components was measured by volume. For resin, we used paper cups, syringe and a beaker for measuring the volume at different times depending on what was available at the moment. For

cobalt and hardener, we used syringe and pipettes. For many batches, cobalt would be already mixed in the resin so one extra step was reduced for us.

Later, we shifted to measurement by weight which enhanced accuracy of measurement of the components. This method did in fact increase accuracy but getting the small weight accurately took multiple attempts which slowed down our working speed. And the measuring device was also at a risk of damage by drips of chemicals. There was a point where to measure very small weight of hardener, we used the volume basis whereas measurement of resin remained mass basis. We had to do that because the measuring device gave inaccurate reading for such small weight. We approximately measured the volume of hardener in given weight and used this method for some time.

After getting a weighting machine with better accuracy we again went back to weight-based measurements for a long time.

While weight basis was productive and accurate it still took a longer to prepare the resin and we could only measure up to 200 gm of weight which did not work for preparing large batches, we started completely volume-based preparation of resin. This way has been very efficient as we can prepare a batch in a shorter time and we could make a batch as large as needed.

Note: Percentage of hardener used can be changed as per requirement from the range 1% to 2%.

1% is best suited when you need to make large pieces in a single attempt or when you have to make complex geometry pieces and require longer working time.

2% can be convenient for when you need to work on small pieces and need the piece to be ready quickly. However, doing this for pieces the size of casting tube can be risky as it compromises the quality of the pieces.

Experiments on molds:

During the first days, our way of making molds was quite inefficient. We would take a pipe or tube of required diameter and apply agar agar gel on the pipe for required length and little extra for tolerance. we would then apply resin on fiberglass like we normally do. After the resin sets, we would cut the resin fiberglass composite in a straight line along the length then separate it from the pipe starting from the place of the cut. we would then seal the cut by applying resin on a strip of fiber cloth along the cut; the width of strip would be large enough to cover the surrounding area of the cut but not too wide to increase the overall diameter of the tube. This Method was highly inconvenient as it put the mold at the high risk of damage during removal of the composite piece and it also created a bulge at the place of cut due to an extra layer used to seal the cut.

Later we started experimenting different method to make molds in a way that it required less steps and ensured that same base pipe could be used multiple times. We used aluminum foil in one such experiment; we would wrap aluminum foil around the circumference of the pipe, apply resin over that and to separate the composite from pipe we would pull it from opposite directions. It partially worked as it did make the removal easy and without any cuts but large bits of aluminum stuck to the inner surface of the composite tube which was a problem. We then started using aluminum foil and taped it in circles along the circumference. This worked really well and we used this method for a while.

The aluminum foil was a good option but it could increase the diameter by 1 or 2 millimeters when paired with tape and it was also costly so we opted for butter paper. Same layering process for butter paper as aluminum foil worked really well. We later experimented with regular A4 paper for small tubes and chart paper for large tubes that we had to make and like before these worked best for us too. Since then, we have been using paper and tape to make molds.

When we can't find a tube to use as a mold due to difference in required and available diameters, we take a smaller tube and wrap it with multiple layers of paper or flex until we get required diameter then we follow the same steps of paper and tape.

For body tube we made rings of plywood and wrapped flex around to get the desired diameter.

2.3. Propellent System and Mechanism

2.4. Aerodynamic Application

To optimize the aerodynamic performance of the rocket and minimize drag, several design and fabrication techniques were applied.

2.4.1. Sanding

The rocket's body parts were fabricated using fiber glass and polyester resin. However, the fabrication process resulted in ridges and surface roughness, which were unacceptable for optimal aerodynamic performance. To address this, the body parts were carefully sanded to achieve a smooth finish. This smooth surface significantly reduced aerodynamic drag, ensuring higher performance and improved flight performance.

2.4.2. Filleting

The rocket's fins were attached to the body using Araldite, a specialized adhesive. Improper application of the adhesive did end up causing irregularities affecting the drag, so to mitigate this, fillets were added at the fin-body joint. A laser-cut jig was used to create precise, curved fillets that minimized airflow separation and reduced drag. The fillets not only enhanced aerodynamic performance and also improved the structural integrity of the fin attachments.

2.4.3. Chamfering

The fins, fabricated from fiberglass, were processed to further optimize their aerodynamic profile. A dedicated setup was prepared for chamfering, where the edges of the fins were shaped into a diamond wedge profile. This chamfered design reduced drag during high-speed flight b streamlining airflow around the fins, contributing to the rocket's stability and performance.

2.5. Flight Electronics and Control System

The avionics system serves as the brain of the Trishul, responsible for monitoring, controlling, and recording critical flight data. It includes multiple sensors, microcontrollers, and communication modules to ensure precise telemetry and ejection mechanism.

Avionics work can be broadly divided into two primary domains: software and hardware. The software aspect primarily involves developing code to control and coordinate the hardware components. On the hardware side, the system comprises a printed circuit board (PCB), a microcontroller, pressure sensors, MOSFETs, and other essential components that enable the overall functionality of the avionics system.

Two distinct PCBs were designed for this project:

1. **The transmitter module**, which was mounted in the rocket's avionics bay and served as the central hub for data acquisition and control.
2. **The receiver module**, which was used on the ground to receive and monitor data during the rocket's flight.

The transmitter module incorporated the following components:

1. Teensy 4.1 Microcontroller (OBC):

The Teensy 4.1 microcontroller is the core of the avionics system. It processes sensor inputs, manages ejection mechanisms, and communicates with the ground station. Its high clock speed and abundant memory make it suitable for real-time data processing and multitasking.

2. MPU6050 Inertial Measurement Unit (IMU):

This IMU measures the rocket's acceleration and angular velocity. By combining data from its accelerometer and gyroscope, the MPU6050 provides real-time orientation and stability feedback.

3. BMP180 Barometric Pressure Sensor:

The BMP180 measures changes in atmospheric pressure to calculate altitude. This sensor is vital for detecting apogee, the highest point in the rocket's flight, which triggers the deployment of the recovery system.

4. NEO-6M GPS Module:

The GPS module provides geolocation data, including latitude and longitude. This component is used for tracking the rocket's position throughout the flight and recovery phases, ensuring the team can locate the rocket post-landing.

5. LoRa RA-02 Communication Module:

The LoRa module enables long-range wireless communication between the rocket and the ground station. It transmits telemetry data such as altitude, orientation, and GPS coordinates in real time.

6. Ejection System:

The ejection system uses IRFZ44N N- type MOSFETs as a switch to control the deployment of recovery parachutes. The system is triggered by the OBC based on altitude data from the BMP180 and also includes redundant timer logic to ensure reliable operation.

7. Indicators (LEDs and Buzzer):

LEDs and a buzzer provide visual and audible status updates. For example, the LEDs indicate power status and readiness, while the buzzer confirms the ejection system's activation or alerts the team during pre-launch checks.

8. Power Interface:

Power is distributed through a XL4016 Step Down Buck Converter 300W 10A, stepping down the 7.4V from the Li-ion batteries to 5V. Resistors are placed strategically for voltage stabilization. To avoid interference or inadequate current affecting the avionics during parachute ejection, a dedicated power supply of two 3.7V, 2200 mAh lithium-ion batteries connected in series was used for the pyro system.

For the receiver module we included the following

1. Arduino Uno:

The Arduino Uno served as the central processor for the ground receiver module, responsible for receiving the data transmitted by the LoRa module on the rocket.

2. LoRa RA-02 Module:

The LoRa module was integrated to establish long-range, low-power communication between the rocket and the ground station.

The primary function of the avionics bay was to measure the rocket's apogee, log GPS, BMP, and MPU data for post-flight analysis, and deploy parachutes for dual recovery. Deployment was triggered either by a detected altitude decrease or after a predetermined time.

To ensure system redundancy and reliability, two additional backup boards were prepared using Arduino Nano and ESP32 microcontrollers. Although these backups were ready for use, the Teensy 4.1 proved fully capable of managing all tasks on its own, thanks to its superior performance.

2.5.1. Code Testing

Each component underwent individual testing to minimize the risk of failure. The final code was developed by integrating these individually tested modules. Initial code testing was performed on a breadboard and later validated on the assembled PCB.

a. Code for Ejection Test

Starting with the BMP180, which was primarily used to measure apogee and control parachute deployment, we began by testing the code for these functions. To simplify PCB design, we developed a custom library named **Teensy_BMP180**, enabling easy use of the secondary I2C port.

Link: https://github.com/SRB-rocketryatpulchowk/Project-Trishul/blob/main/Test%20codes/Ejectiontestcode.ino

Using the custom library, we proceeded to develop and test the code for parachute ejection.

Link: https://github.com/SRB-rocketryatpulchowk/Project-Trishul/tree/main/libraries/Teensy_BMP_180

This code differed from the final version in its use of two MOSFETs to control the ejection of the drogue and main parachutes, with a specific time delay between the two deployments.

b. Code for launch detection

Next, we integrated the **MPU6050** to detect the launch, which was a critical event for starting the timer. This timer acted as a redundancy measure in case the BMP180 failed due to unforeseen circumstances.

To ensure the code executed swiftly, we avoided implementing any filters that could slow down processing. Consequently, we had to carefully consider the threshold values, as the raw data being used inherently contained significant noise and errors.

Link: https://github.com/SRB-rocketryatpulchowk/Project-Trishul/blob/main/Test%20codes/laundetection.ino

c. Code for GPS initialization and activation

Next, we integrated the GPS module to ensure the rocket could be located in case it drifted beyond the expected range.

Link: https://github.com/SRB-rocketryatpulchowk/Project-Trishul/blob/main/Test%20codes/GPSinitializationandactivation.ino

d. Code for LORA transmitter and receiver module

We utilized the LoRa module for real-time communication, enabling us to monitor the apogee and receive updates on launch detection without needing to open the avionics bay or analyze the SD card data.

For testing, the receiver module was configured to transmit GPS data and BMP readings.

Link: https://github.com/SRB-rocketryatpulchowk/Project-Trishul/blob/main/Test%20codes/LORAtransmitter.ino

For testing, the receiver module was configured to transmit GPS data and BMP readings.

Link: https://github.com/SRB-rocketryatpulchowk/Project-Trishul/blob/main/Test%20codes/LORAreceiver.ino

No further changes were necessary for the final version of the receiver module code.

e. Final code

Finally, we moved on to combining the individually tested codes, making the necessary adjustments. We integrated buzzers, the SD card, and made modifications to the ejection code for dual deployment and the timer. These changes were made based on our evolving needs and were quite frequent. Ultimately, we arrived at the following final code:

Link: https://github.com/SRB-rocketryatpulchowk/Project-Trishul/blob/main/Final%20codes/Finalcode.ino

2.5.2 Hardware Design and Fabrication

Schematic Development: The circuit design and schematic focused on creating a robust and efficient avionics system for the rocket. It incorporated a Teensy 4.1 microcontroller as the main OBC, with sensors (MPU6050, BMP180, and NEO-6M GPS) and a LoRa RA-02 module for telemetry.

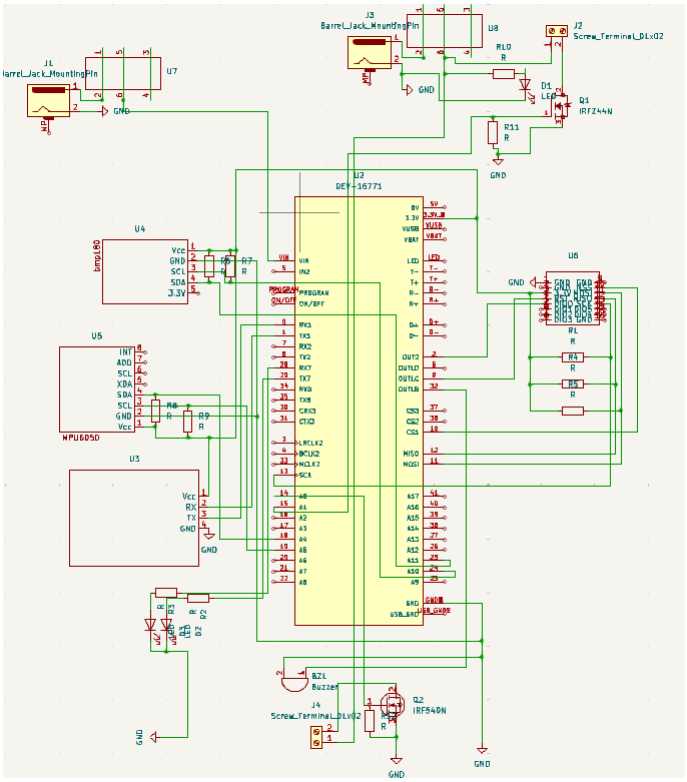

Fig 2.5.2.1: Schematic diagram

Prototyping and Testing: Breadboard testing was conducted for individual subsystems before assembling the final PCB.

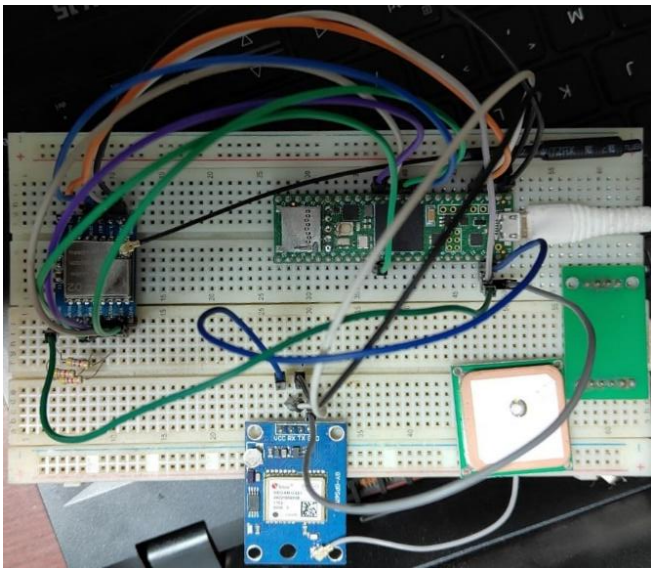

Fig 2.5.2.2: Breadboard testing

Final PCB Design: The schematic from the design phase was converted into a PCB layout using KiCad software. A single-layer PCB was used to accommodate the routing of signals, power, and ground traces.

Different PCB designs were tested and the final one is as shown in the figure below. The different PCB designs that we tried before finalizing the designs are all present in the Github link below

Link: https://github.com/SRB-rocketryatpulchowk/Project-Trishul/tree/main/PCB%20Designs

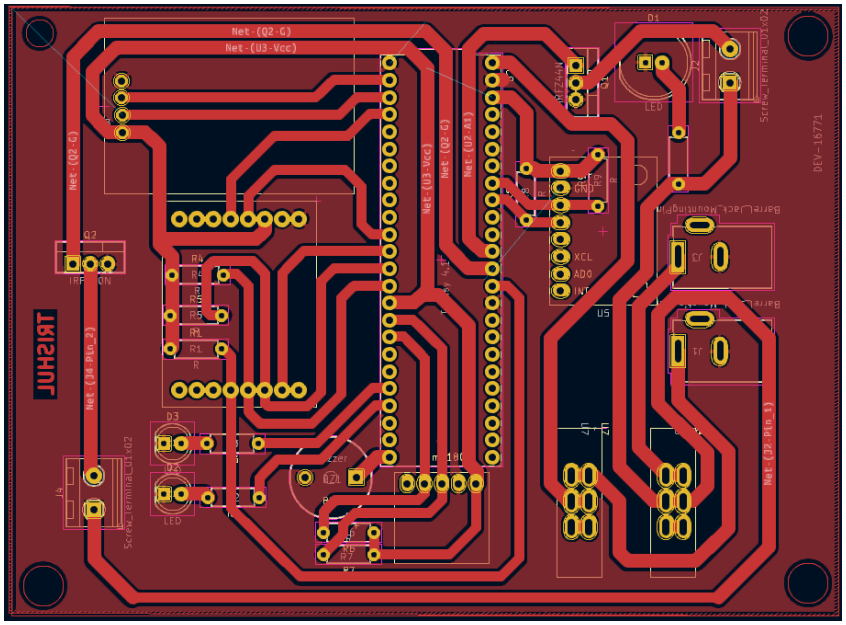

Fig 2.5.2.3: Final PCB design

Fabrication Process: The fabrication of the PCB was carried out using a single-sided copper-clad board. The step-by-step process is detailed below:

I. **PCB Design**: The circuit design was created using **KiCAD** software. The layout was planned based on the required dimensions of the electronic components.
II. **Printing the Design**: A PCB design was printed on specialized transfer paper i.e. Glossy Photo Paper.
III. **Copper Board Preparation**: The copper-clad board was cleaned thoroughly with stainless steel scrubber to remove any oxidation or contaminants, ensuring a clean surface for the transfer process.
IV. **Design Transfer**: The printed side of the transfer paper was carefully aligned with the copper board. An iron was used as laminator to apply heat and pressure, transferring the toner onto the copper board to form the circuit pattern.

V. **Cooling and Peeling**: After the board cooled down, the transfer paper was gently peeled off, leaving the toner firmly adhered to the copper board, accurately representing the circuit design.

VI. **Etching Process**: The board was immersed in an etching solution made of hydrochloric acid (HCl) and hydrogen peroxide (H_2O_2) in a 1:3 ratio. This dissolved the exposed copper, leaving only the protected traces as per the design.

VII. **Cleaning and Inspection**: The toner was removed using scrubber to reveal the copper traces. The board was then cleaned thoroughly and inspected for any flaws or incomplete etching.

VIII. **Drilling and Finishing**: Holes for component leads and mounting were drilled into the board with 1mm drill bit. Care was taken to ensure the drilled holes were aligned correctly with the design

IX. **Component Soldering**: Components were soldered onto the PCB using soldering iron and solder wire. Special attention was given to ensure strong and reliable solder joints while avoiding short circuits.

After successful fabrication, code testing and assembling the components together the avionics bay appeared as shown below

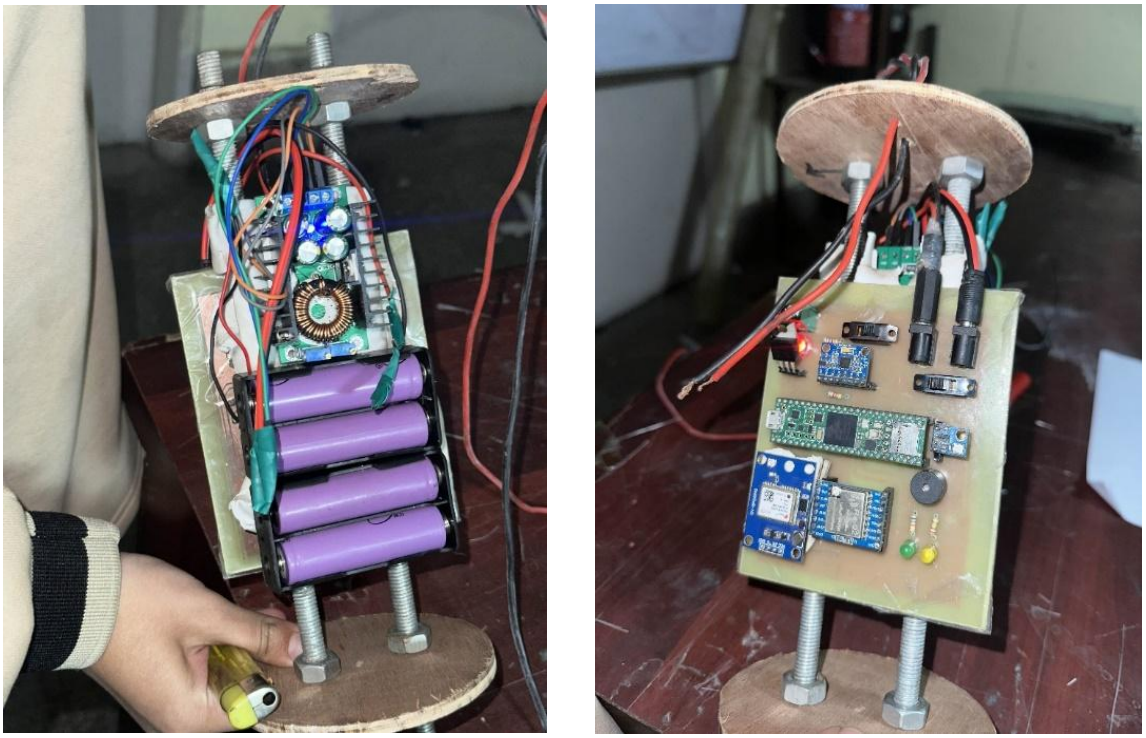

Fig 2.5.2.4: Final Avionics Bay(front and back)

Potential Areas of Failure:

Despite rigorous design and testing, the following areas were identified as potential weak points in the avionics system which were solved and amended by multiple testing:

- Power Supply Reliability:
  When all the sensors in the system were powered by the same power supply along with the ejection system, voltage dropped during high current demand from ejection system and the supply was inadequate to the OBC to operate. We resolved the issue by providing dedicated power supply to both OBC and ejection system.

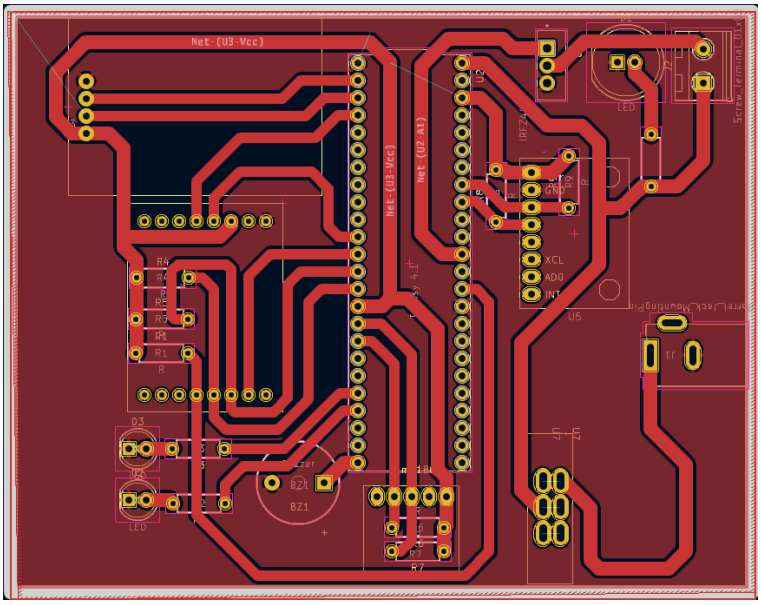

Fig 2.5.2.5: Solution for better power supply reliability

- Sensor Calibration Drift:
  We noticed that environmental conditions could cause sensors like the BMP180 to drift. When the sensor was tested under the sunlight or at night, the ejection itself got triggered. We noticed that the altitude data given by the sensor had negative value which triggered the ignition untimely. In order to mitigate this, we used a black tape to cover the BMP 180 while testing under the sunlight.

- PCB Designs: Multiple failed PCB designs were made during the attempt to make our final PCB board. Inaccurate size of footprints for the sensors, unreliable soldering, lacking the use of pull-up and pull-down resistors were the common problems that we faced in the failed designs. The problems were identified during the fabrication and

testing phase where we thoroughly studied them and mitigated it according to the requirements.

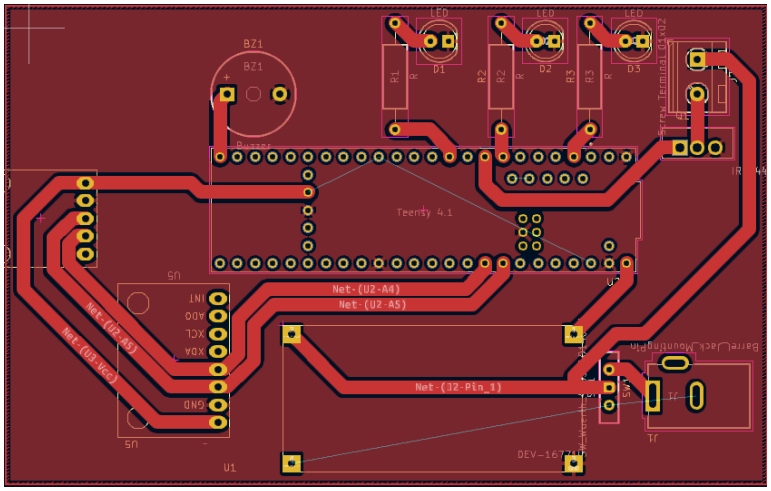

Fig 2.5.2.6:

- Prolonged Initialization of GPS module:
  The GPS module (NEO-6M) experienced significant delays in obtaining a GPS fix, particularly during initial setup. We could see the delays in cold start conditions, where the GPS requires downloading satellite data from scratch. Therefore, the system was pre-tested in open environments to ensure faster satellite lock during actual deployment.

- LoRa Communication Issues:
  During testing, it was observed that the LoRa module (RA-02) occasionally failed to transmit all data packets reliably. This led to incomplete data reception at the ground station, potentially caused by environmental interference, range limitations, bandwidth constraints or transmission delays.

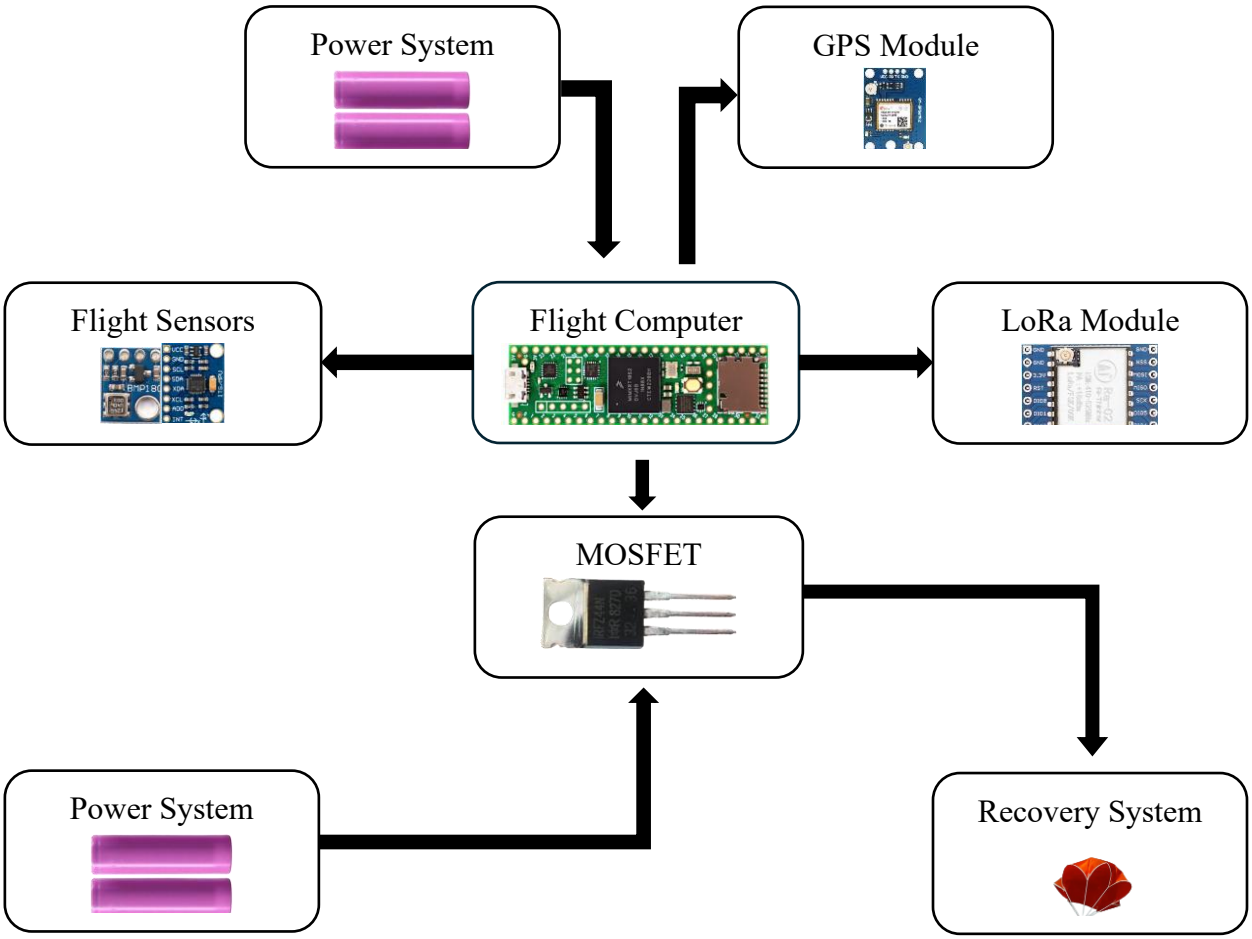

Fig 2.5.2.7: Flowchart of the avionics system

2.6. Recovery system

The parachute is a very essential component of the rocket, playing an important role in ensuring a safe and controlled recovery after flight. Its main purpose is to reduce the rocket's descent speed, reducing the forces acting on the rocket during the decent and preventing damage to both the rocket and its payload. For this project, we utilized a dual-parachute recovery system consisting of a main parachute and a drogue parachute, both of which are equally important functions. The drogue parachute is responsible for stabilizing the rocket immediately after apogee, controlling its orientation and descent rate during the initial phase of recovery. The main parachute, deployed at a lower altitude, significantly slows the rocket for a soft landing.

2.6.1. Parachute selection

To select a parachute that meets our requirements, we first calculated the drag coefficient (Cd) of the available parachutes to determine whether they could support the weight of the final rocket.

After determining the C_d, it was crucial to evaluate the terminal velocity of the parachutes when used with the final rocket body. The terminal velocity needed to strike a balance: it should not be too high, as that would reduce the cushioning effect upon landing, nor too low, as it could cause the parachute to drift excessively due to wind. Therefore, the ideal terminal velocity was determined to be approximately 6–7 m/s.

We tested three available parachutes and calculated the Cd of each using two methods:

1. Drop testing
2. Wind tunnel testing

The equation used for this calculation is as follows:

$$F = \frac{1}{2}\rho v^2 A C_d$$

$$where, F = Weight\ of\ the\ test\ object$$

$$\rho = density$$

$$v = terminal\ velocity$$

$$A = reference\ area$$

$$C_d = coefficient\ of\ drag$$

As mentioned earlier we

1) From Drop test,

a) Black Parachute

$Reference\ Area = 1.2025\ m^2$

$Average\ time\ for\ drop = 3.24s$

$height\ of\ drop = 43ft = 13.1064m$

$Velocity = \frac{13.1064}{3.24}\ m/s$

$= 4.0451\ m/s$

$Therefore\ we\ get\ , C_d = \frac{2W}{\rho v^2 A}$

$= \frac{2 \times 9.81 \times 0.874}{1.225 \times 4.0451^2 \times 1.2025}$

$= 0.771$

If we were to use the black parachute as the parachute for the final body then,

Terminal velocity of the parachute for the 15 kgs, $v = \sqrt{\frac{2 \times 9.81 \times 15}{1.225 \times 1.2025 \times 0.711}}$

$$or, v = 16.76\ m/s$$

b) Pink Parachute

$Reference\ Area = 1.4625\ m^2$

$Average\ time\ for\ drop = 3.338s$

$height\ of\ drop = 42\ ft = 12.8016m$

$Velocity = \frac{12.8016}{3.338}\ m/s$

$= 3.835\ m/s$

$Therefore\ we\ get\ , C_d = \frac{2W}{\rho v^2 A}$

$= \frac{2 \times 9.81 \times 0.874}{1.225 \times 3.835^2 \times 1.4625}$

$= 0.65$

If we were to use the pink parachute as a parachute for the final body then,

Terminal velocity of the parachute for the 15 kgs, $v = \sqrt{\frac{2\times9.81\times15}{1.225\times1.4625\times0.65}}$

$$or, v = 15.89\, m/s$$

c) Red parachute

$Reference\ Area = 5.46\, m^2$

$Average\ time\ for\ drop = 6.133s$

$height\ of\ drop = 38.50\, ft = 11.737m$

$Velocity = \frac{11.737}{6.1333}\ m/s$

$= 1.91365\ \ m/s$

$Therefore\ we\ get\ , C_d = \frac{2W}{\rho v^2 A}$

$= \frac{2 \times 9.81 \times 0.874}{1.225 \times 3.3745^2 \times 5.46}$

$= 0.702$

If we were to use the red parachute as a parachute for the final body then,

Terminal velocity of the parachute for the 15 kgs, $v = \sqrt{\frac{2\times9.81\times15}{1.225\times\times0.702}}$

$$or, v = 7.91\, m/s$$

2) From wind tunnel testing,

In this method the total force exerted was measured using a spring balance and velocity was measured at the intersection of point of canopy and the string.

The string length was kept 1.5 times the diameter of the parachute.

a) Black Parachute

$Reference\ Area = 1.2025\, m^2$

$Force = 0.75 \times 9.81\ N$

$Average\ velocity = 3.56\ m/s$

$Therefore\ we\ get\ , C_d = \frac{2F}{\rho v^2 A}$

$= \frac{2 \times 9.81 \times 0.75}{1.225 \times 3.56^2 \times 1.2025}$

$= 0.789$

If we were to use the black parachute as a parachute for the final body then,

Terminal velocity of the parachute for the 15 kgs, $v = \sqrt{\frac{2 \times 9.81 \times 15}{1.225 \times 1.2025 \times 0.789}}$

$$or, v = 14.23 m/s$$

b) Pink Parachute

$Reference\ Area = 1.4625\ m^2$

$Force = 1 \times 9.81\ N$

$Average\ velocity = 3.71\ m/s$

$Therefore\ we\ get\ , C_d = \frac{2F}{\rho v^2 A}$

$= \frac{2 \times 9.81}{1.225 \times 3.71^2 \times 1.4625}$

$= 0.79$

If we were to use the pink parachute as a parachute for the final body then,

Terminal velocity of the parachute for the 15 kgs, $v = \sqrt{\frac{2 \times 9.81 \times 15}{1.225 \times 1.4625 \times 0.79}}$

$$or, v = 14.42 m/s$$

c) Red Parachute

$Reference\ Area = 5.46\ m^2$

$Force = 2 \times 9.81\ N$

$$Average\ velocity = 2.805\ m/s$$

$$Therefore\ we\ get\ , C_d = \frac{2F}{\rho v^2 A}$$

$$= \frac{2 \times 9.81 \times 2}{1.225 \times 2.805^2 \times 5.46}$$

$$= 0.745$$

If we were to use the red parachute as a parachute for the final body then,

Terminal velocity of the parachute for the 15 kgs, $v = \sqrt{\frac{2 \times 9.81 \times 15}{1.225 \times 5.46 \times 0.745}}$

$$or, v = 7.681 m/s$$

Based on the calculated values of Cd and terminal velocity, we selected the pink parachute to serve as the drogue parachute and the red parachute as the main parachute for our dual-deployment system.

2.6.2 Shock Cord

The shock cord holds the parts of the rocket together after they separate at ejection. The shock cord may be made of an elastic material to help absorb the shock of the separating parts coming to a halt at the ends of the cord, or it could be made from a non-elastic line (in which case it is normally longer). Typical materials for shock cards are sewing elastic, rubber, nylon, and Kevlar.[3]

We were unable to experimentally determine the shock force that the shock cord would experience. Based on previous projects, we selected an elastic shock cord in combination with a metal chain. The metal chain was directly attached to the separation plate to ensure it was pulled out during parachute ejection when the black powder charge ignited.

As we planned for dual ejection to take place one of the parachutes, the main parachute was folded and kept in the nose cone and the drogue parachute was kept between the avionics bay and the engine block. The shock chord was to keep these parts together.

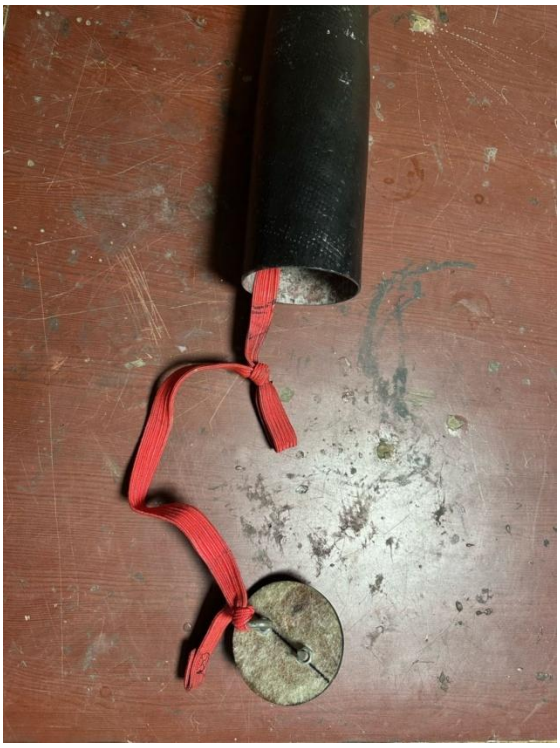

Fig 2.6.2.1. Shock chord connecting to the nose cone

Fig 2.6.2.2 shock chord connecting to the engine block and avionics bay

2.6.3 Ejection System

The ejection system used IRFZ44N N- type MOSFETs as a switch to control the deployment of recovery parachutes. The system is triggered by the OBC based on altitude data from the BMP180 and also includes redundant timer logic to ensure reliable operation.

When the switch was turned on, power from the batteries was directed to ignite a small piece of Nichrome wire, which was fitted inside a canister, as shown in the photo.

The canisters were packed with approximately 5 grams of black powder and sealed tightly with foam and tape. When ignited, the black powder would generate pressure within the nose cone and body tube, causing them to separate and deploying the parachute as intended.

Fig.2.6.3.1: Black powder containing canisters

The nose cone would separate to deploy the drogue parachute and the body tube to deploy the main parachute.

2.6.4 Packing the Parachutes for Deployment

The success of recovery largely depends on how the parachutes are packed. To ensure they deploy smoothly after ejection, we experimented with various packing methods. The most reliable method is detailed below:

First, the parachute canopy was fully spread out on the ground with the suspension lines neatly arranged on one side. The canopy was then folded in half lengthwise, ensuring the edges were aligned. This process of folding in half was repeated multiple times until the parachute formed a narrow strip. Once the canopy was folded into a thin line, it was rolled along the straight line formed, like rolling a duvet. We then had a small ball or roll of the parachute, which was then carefully placed into the rocket.

Fig 2.6.4.1: Folding the parachutes

The parachute was folded and refolded several times, with one team member running while holding the parachute to test the deployment and to verify that it unfolded correctly during descent. Through the repeated trials, we experimented with different folding techniques and the number of rolls was changed in each trial to find the perfect number we needed for the deployment. These tests were crucial in identifying the perfect folding technique and achieving the desired parachute opening time required for safe recovery.

2.7 Launch Stand

The launch stand was designed and constructed to achieve optimal stability and performance during the rocket launch process. This assembly features three iron rods strategically arranged in a symmetrical configuration at 120-degree angles, converging at the top to create an equilateral triangular framework. This triangular design not only enhances the structural integrity of the assembly but also provides a balanced support system that is crucial for maintaining the rocket's stability during ignition and launch.

The triangular structure, also fabricated from high-strength iron rods, serves as the backbone of the launch pad, ensuring that the rocket remains securely positioned and properly aligned throughout the launch sequence. This careful engineering minimizes the risk of any wobbling or misalignment that could compromise the integrity of the launch.

To further reinforce the assembly, the base of the launch pad is constructed with a durable plywood platform. This platform is designed to withstand the considerable forces exerted during ignition and launch, providing a stable foundation that enhances the overall reliability of the launch setup. The combination of the iron rod framework and the plywood base creates a robust system capable of handling the dynamic stresses associated with rocket launches.

Moreover, this carefully setup facilitates precise alignment, allowing for accurate positioning of the rocket. Ensuring that the rocket is securely supported throughout the launch sequence is paramount, as it contributes to the overall success of the mission. The attention to detail in the design and construction of the launch rod assembly exemplifies our commitment to excellence in aerospace engineering, reflecting our dedication to safety, stability, and performance in every aspect of the launch process.

2.8 Launch Controller

The launch controller was engineered to prioritize safety, functionality, and reliability throughout the entire rocket launch process. A key feature of this design is a toggle switch dedicated to testing the continuity of the ignitor circuit. This crucial component allows operators to verify the integrity of the circuit prior to ignition. When the circuit is confirmed to be continuous, a red LED indicator lights up, accompanied by an audible alert from a buzzer, thereby confirming the system's readiness for ignition. This dual feedback mechanism not only enhances operational clarity but also instills confidence in the safety protocols being followed.

To further enhance safety, the continuity circuit is powered by a 9-volt battery, a deliberate choice that ensures the rocket cannot ignite during the continuity test. This precaution is essential in preventing any unintended ignition during critical pre-launch checks. For the ignition system itself, a separate 19-volt battery is utilized, and the two circuits are interconnected in such a

manner that ignition can only occur after the successful completion of the continuity test and the subsequent connection of the 19-volt battery. This thoughtful design philosophy reinforces the reliability and operational integrity of the launch controller.

The ignition system incorporates a dual-safety mechanism consisting of two switches: a toggle switch and a push button. Both switches must be activated simultaneously to initiate the launch sequence, effectively preventing the risk of accidental ignition. This design philosophy underscores our commitment to safety, ensuring that the rocket cannot be ignited inadvertently.

In addition, the controller features a two-pin connector designed for seamless integration between the launch system and the rocket. This connector allows the wires from the rocket's ignitor to be securely attached, facilitating a straightforward and efficient connection that minimizes the potential for errors during setup.

Moreover, the controller facilitates the remote activation of the ignitor by delivering a controlled electrical current necessary for igniting the rocket motor. This capability enables the launch team to maintain a safe distance from the rocket during the ignition process, significantly enhancing operational safety and minimizing risk.

Safety interlocks, such as the dual-switch activation requirement, the two-pin connector, and the use of separate power sources for the continuity and ignition circuits, provide additional layers of security.

These interlocks are instrumental in preventing unauthorized or unintended ignition attempts, ensuring that all operational protocols are followed.

In conclusion, the combination of these advanced features renders the launch controller a precise, secure, and effective tool for igniting the rocket motor during the launch process. By integrating robust safety measures with reliable functionality, we uphold the highest standards of safety and performance in aerospace operations. This thoughtful engineering not only reflects our dedication to excellence but also contributes to the overall advancement of aerospace technology, ensuring a successful and secure launch experience for all involved.

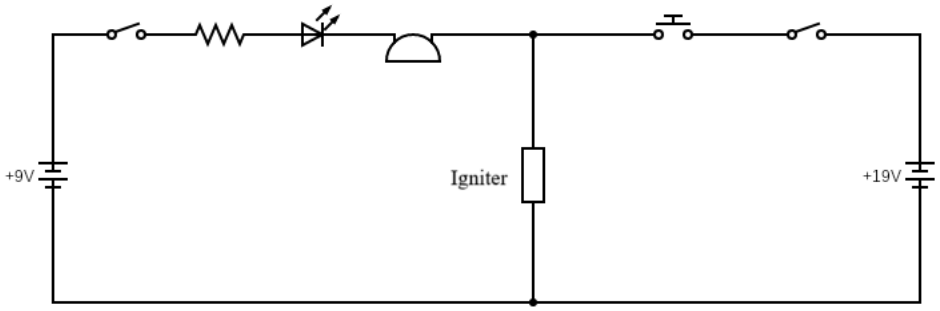

Fig 2.8.1: Launch Controller Circuit

3. Results and Discussions

3.1. Final assembled Body

After months of continuous hard work and dedication, our project reached its final stage. With the assembly of all components complete, our rocket was ready for launch.

Fig 3.1.1: Final assembled body

3.2. Flight test:

On January 4, 2025, Trishul underwent a test flight targeting an apogee of 3000 meters. The rocket's configuration utilized standard electronic systems, including a flight computer, SD card for data storage, BMP 180 and MPU 6050 sensors, a Lo-Ra module, a GPS module, and power supplies. Following a vertical launch, the rocket reached an apogee of 2612 meters, maintaining stable flight dynamics. The ejection system successfully initiated at the intended altitude, with the deployment charge firing at the precise moment to separate the recovery system. The parachute deployed correctly upon ejection, aided by a shock cord, enabling a controlled descent. Despite minor structural stress during landing, the rocket remained largely intact, allowing full

retrieval of all onboard components and flight data. This flight demonstrated the effectiveness of the recovery system's timing and parachute activation, marking a critical milestone in the project's development.

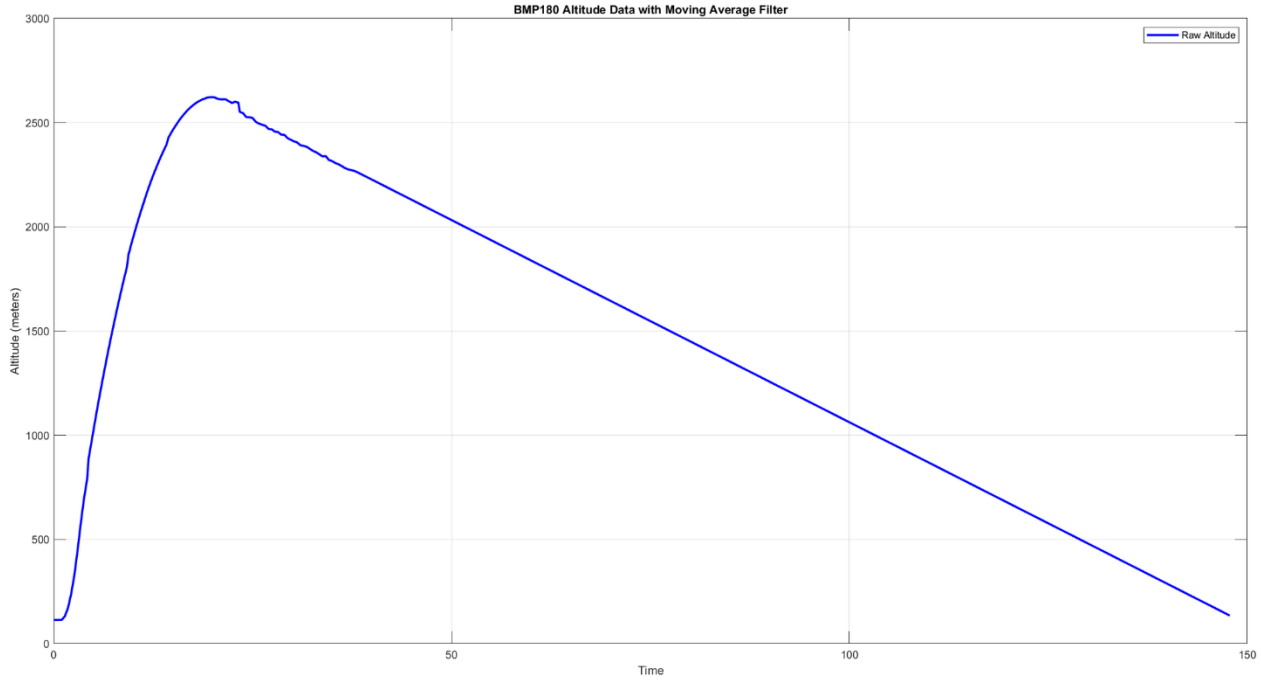

Fig.3.2.1: Post Processed BMP data

The graph illustrates the altitude profile of the rocket over time, recorded using a BMP180 pressure sensor. The steep ascent curve reflects strong acceleration at launch, with the rocket reaching a peak altitude of approximately 2600 meters. The apogee transition appears relatively smooth, with minor fluctuations likely due to sensor noise or ejection charge. The descent phase follows a steady downward trajectory, indicating a parachute-controlled recovery. The rate of descent suggests that the dual parachute system deployed successfully, preventing a ballistic return.

Comparison between the actual graph (Fig 3.2.1) and the simulated one (Fig 2.1.5.)

The graph in **Fig 3.2.1** is the real flight data recorded from the BMP180 sensor, and the **Fig 2.1.5.** graph is a simulated ideal of how the rocket was supposed to fly. What is amazing about this comparison is how well the real-world output compares to the simulated profile. The altitude achieved—about 2650 meters for actual data versus just over 2700 meters for simulation—is remarkably close, considering the real flight involves uncontrollable

variables like wind, minor launch angle variations, sensor noise, and environmental conditions. In spite of these challenges, actual data duplicates the shape and direction of the simulated curve: a clean climb, a clear apogee, and an smooth fall.

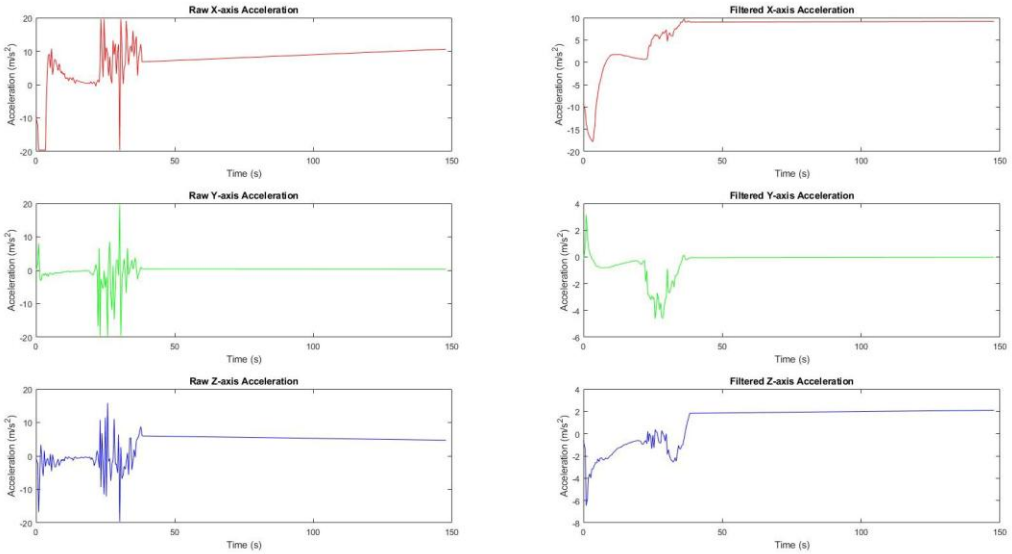

Fig 3.2.2: Post processed MPU data

The set of graphs represents the raw and filtered acceleration data along the X, Y, and Z axes during the rocket's flight. The raw acceleration data shows high-frequency noise and fluctuations, especially in the initial phase of the flight, likely due to launch vibrations and environmental disturbances. The X-axis acceleration exhibits sharp spikes, indicating sudden forces applied during launch and possible disturbances during the powered ascent. The Y and Z axes also display high variability, particularly in the early phase, which could be due to aerodynamic forces and roll instability.

After applying a filter, the noise is significantly reduced, revealing a smoother acceleration trend. The filtered data provides a clearer view of the transition from powered ascent to coasting, confirming a successful motor burn phase. The acceleration gradually decreases as the thrust phase ends, and the rocket enters free flight. The refined data also reveals more accurate peak acceleration values and helps in determining the exact moments of events such as burnout and apogee.

4. Recommendations

For future projects to turn out even better in the future, the Team SRB-2024 would like to recommend the following:

1) To calibrate the MPU6050 accelerometer in the final code to obtain more accurate data for post-processing.
2) To use GPS modules and LORA modules like
   for better navigation and smoother communication
3) To use timestamps with millisecond precision to aid in post-processing.

5. Conclusion

Hence, the project almost met its main goals of developing and flight-testing a solid-fuel rocket aimed at an altitude of 3000 meters, implementing effective recovery systems, and gathering flight data for refinement in the future. The results offer a practical foundation for enhancing propulsion efficiency, structural development, and recovery methods, in addition to encouraging further innovation through lessons learned and recorded concepts.

6. References

[1] "Beginner's Guide to Rockets." Accessed: Apr. 30, 2025. [Online]. Available: https://www.grc.nasa.gov/www/k-12/rocket/bgmr.html

[2] "Solid rocket booster - Wikipedia." Accessed: Apr. 30, 2025. [Online]. Available: https://en.wikipedia.org/wiki/Solid_rocket_booster

[3] "Model Rocket Parts." Accessed: Apr. 29, 2025. [Online]. Available: https://www.unm.edu/~tbeach/IT145/week05/parts.html